Acta Crystallographica Section F
Structural Biology Communications
ISSN 2053-230X

Preliminary joint X-ray and neutron protein crystallographic studies of ecDHFR complexed with folate and NADP$^+$

Qun Wan,[a]* Andrey Y. Kovalevsky,[b] Mark A. Wilson,[c] Brad C. Bennett,[d] Paul Langan[b] and Chris Dealwis[e]*

[a]Department of Biochemistry, College of Medicine, Yangzhou University, 11 HuaiHai Road, Yangzhou 225001, People's Republic of China, [b]Biology and Soft Matter Division, Oak Ridge National Laboratory, PO Box 2008, Oak Ridge, TN 37831, USA, [c]Department of Biochemistry/Redox Biology Center, University of Nebraska, 1901 Vine Street, Lincoln, NE 68588, USA, [d]Department of Molecular Physiology and Biological Physics, University of Virginia, PO Box 800793, Charlottesville, VA 22908, USA, and [e]Department of Pharmacology, Case Western Reserve University, 10900 Euclid Avenue, Cleveland, OH 44106, USA

Correspondence e-mail: wqun@yzu.edu.cn, cxd114@case.edu

Received 8 April 2014
Accepted 26 April 2014

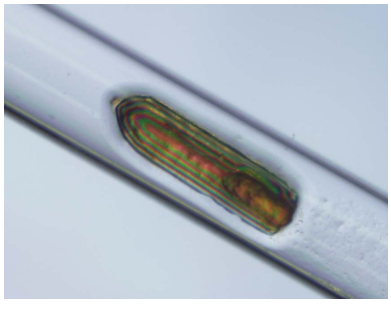

A crystal of *Escherichia coli* dihydrofolate reductase (ecDHFR) complexed with folate and NADP$^+$ of 4 × 1.3 × 0.7 mm (3.6 mm^3) in size was obtained by sequential application of microseeding and macroseeding. A neutron diffraction data set was collected to 2.0 Å resolution using the IMAGINE diffractometer at the High Flux Isotope Reactor within Oak Ridge National Laboratory. A 1.6 Å resolution X-ray data set was also collected from a smaller crystal at room temperature. The neutron and X-ray data were used together for joint refinement of the ecDHFR–folate–NADP$^+$ ternary-complex structure in order to examine the protonation state, protein dynamics and solvent structure of the complex, furthering understanding of the catalytic mechanism.

1. Introduction

Dihydrofolate reductase (DHFR) is an NADPH-dependent enzyme that catalyzes the reduction of 7,8-dihydrofolate (DHF) to 5,6,7,8-tetrahydrofolate (THF), which is required in the biosynthesis of purine, thymine and several amino acids (Sawaya & Kraut, 1997; Reyes *et al.*, 1995; Chen *et al.*, 1994). In rapidly proliferating cells, DNA synthesis greatly increases the demand for dNTPs. THF is the one-carbon carrier during dNTP synthesis. Hence, DHFR is a drug target for cancer, malaria and rheumatoid arthritis to inhibit cell proliferation (Yuthavong *et al.*, 2012; Sharma & Chauhan, 2012; Schweitzer *et al.*, 1990).

During reduction of DHF, a proton is donated to the N5 atom of the DHF pterin ring with a hydride transfer occurring from the nicotinamide ring of NADPH to the C6 atom of DHF. Previously, several catalytic mechanisms have been proposed based on experimental and theoretical studies of DHFR (Shrimpton & Allemann, 2002; Cummins & Gready, 2001; Falzone *et al.*, 1994; Chen *et al.*, 1994; Bajorath *et al.*, 1991). Most of these mechanisms involve a proton relay that includes the catalytic Asp27, a structurally conserved water molecule and the O4 atom of the pterin ring, which may tautomerize from the keto to the enol form during catalysis. Some mechanisms invoke a second water molecule to be directly involved in the protonation of the N5 atom (Chen *et al.*, 1994; Shrimpton & Allemann, 2002). Cummins & Gready (2001) have proposed that hydride transfer from the nicotinamide C4 atom of NADPH to the C6 atom of DHF occurs synchronously with the protonation of N5 to convert DHF to THF (Cummins & Gready, 2001). It is generally proposed that the deprotonated Asp27 is particularly important for the increase in the value of pK_a of the N5 atom of the substrate from 2.4 to 6.5 (Khavrutskii *et al.*, 2007; Chen *et al.*, 1994; Bajorath *et al.*, 1991; Maharaj *et al.*, 1990; Fig. 1). The ability to differentiate between the mechanisms proposed above is limited because the protonation states of the ligand and catalytic residues are difficult to determine using X-ray crystallography even at atomic resolution (Fisher *et al.*, 2012).

Neutron crystallography (NC) can be used to locate H atoms and can readily provide information on the protonation states of amino-acid residues and ligands, the identity of solvent molecules and the nature of bonds involving hydrogen (Niimura & Bau, 2008; Blakeley *et al.*, 2008; Niimura, 1999). In addition, NC can also be used to study protein dynamics by analyzing the backbone amide hydrogen/deuterium-exchange (HDX) pattern: higher exchange rates have been correlated to higher dynamics (Sukumar *et al.*, 2010; Bennett *et*

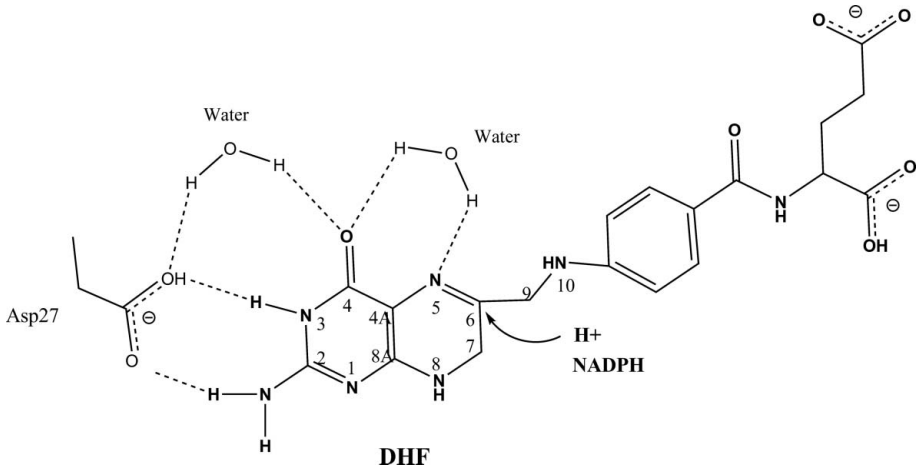

Figure 1
A proposed mechanism of dihydrofolate (DHF) reduction. The N5 atom of folate might be directly protonated by a neighboring water molecule. Another proposed mechanism involves a proton relay from the catalytic Asp27 to a water molecule and the tautomerized O4 atom of DHF. Hydride transfer occurs from NADPH to the C6 of DHF to convert DHF to tetrahydrofolate (THF).

al., 2006, 2008). To understand the catalytic mechanism of DHFR, it is imperative to visualize both H atoms and protein dynamics. Therefore, H atoms, which are normally invisible in X-ray crystal structures of DHFR, should become visible in neutron structures.

Here, we report the crystallization of *Escherichia coli* DHFR (ecDHFR) in complex with folate and $NADP^+$. As folate is a slow-turnover substrate and $NADP^+$ is inactive, the ecDHFR–folate–$NADP^+$ complex has been considered to be a pseudo-Michaelis complex useful for the understanding of the catalytic mechanism of DHFR (Falzone *et al.*, 1994; Reyes *et al.*, 1995; Sawaya & Kraut, 1997; Bhabha *et al.*, 2011). We obtained a ~3.6 mm^3 (4 × 1.3 × 0.7 mm) crystal by optimizing the *de novo* crystallization conditions, followed by microseeding and macroseeding techniques. A 2.0 Å resolution neutron data set was collected with 79.3% completeness on the IMAGINE beamline (Meilleur *et al.*, 2013) located at the High Flux Isotope Reactor (HFIR) within Oak Ridge National Laboratory, Oak Ridge, Tennessee, USA. A 1.6 Å resolution room-temperature X-ray data set was also collected from a smaller crystal harvested from the same crystallization condition. Both data sets were used for joint X-ray/neutron (XN) refinement (Afonine *et al.*, 2010) to study the reaction mechanism of DHFR.

2. Materials and methods

2.1. Protein expression and purification

E. coli DHFR (ecDHFR) was cloned, expressed and purified using the previously described protocol for the recombinant production of *Bacillus anthracis* DHFR (Bennett *et al.*, 2007). Briefly, the cDNA of ecDHFR was cloned into a pET-SUMO vector (Invitrogen) with SUMO and a 6×His tag at the exact N-terminus of the construct. The advantage of this fusion protein system is that, after cleavage, no exogenous residues are left on the target protein. After expression in competent *E. coli* BL21(DE3) cells, the protein was extracted using sonication and centrifugation. The His-tagged protein was purified *via* immobilized metal-affinity chromatography (IMAC) using a nickel column. Next, the SUMO protease from yeast, Ulp1, was added to the purified fusion protein to remove SUMO and the His tag. The protease-treated protein mixture was loaded onto a new nickel-affinity column and the flowthrough contained the pure wild-type ecDHFR (Fig. 2). Because of its poor solubility, folate was added to ecDHFR at a molar ratio of 3:1 when the protein was at only 1 mg ml^{-1} (Sawaya & Kraut, 1997). After concentration to 30 mg ml^{-1}, $NADP^+$ was added to the protein solution at a molar ratio of 3:1 and the protein was further concentrated to 40 mg ml^{-1}. The solution of the concentrated protein complex (ecDHFR–folate–$NADP^+$) was clarified at 15 000*g* for 45 min, aliquoted and stored at −80°C.

2.2. Crystallization

The ecDHFR–folate–$NADP^+$ complex was crystallized *de novo* using the hanging-drop method at 4°C: 1 µl protein solution was added to 1 µl reservoir solution (18% PEG 400, 100 m*M* $MnCl_2$, 20 m*M* imidazole pH 7.0). Crystals appeared in 1 d and continued to grow for 5 d until they reached their largest dimensions. Although the crystallization condition was optimized, most of the crystals were still not single and formed dense clusters (Fig. 3*a*). Hence, the micro-

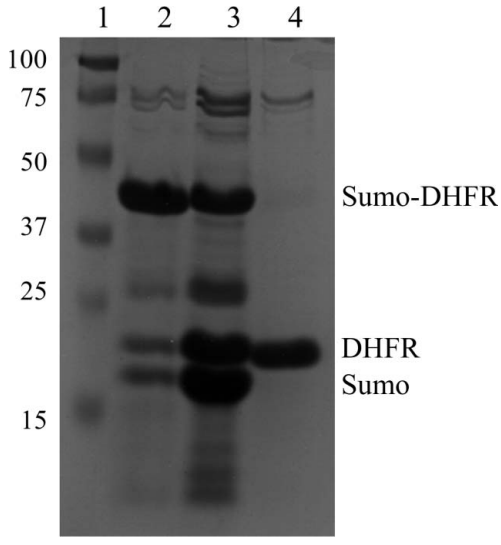

Figure 2
Purification of ecDHFR. After two-step purification using IMAC, ecDHFR can be obtained with more than 90% purity. Lane 1, protein markers (labeled in kDa). Lane 2, fusion protein from the first step of purification. Lane 3, Ulp1 protease-treated protein mixture. Lane 4, wild-type ecDHFR after the second purification.

seeding technique (Bergfors, 2003) was applied to obtain single crystals using a cat whisker in the following condition: 15%(*v*/*v*) PEG 400, 100 m*M* $MnCl_2$, 20 m*M* imidazole pH 7.0. The size of these resultant crystals was usually 1.5 × 0.1 × 0.2 mm (∼0.03 mm^3; Fig. 3*b*), which is too small for neutron diffraction (Blakeley *et al.*, 2008; Bennett *et al.*, 2005). To obtain a crystal of >1 mm^3 in size and to reduce the data-collection time, the macroseeding technique (Bergfors, 2003) was applied. A small single crystal was picked from the original crystallization drop and transferred to 2 µl washing solution [20%(*v*/*v*) PEG 400, 100 m*M* $MnCl_2$, 20 m*M* imidazole pH 7.0]. After four consecutive rounds of washing using the washing solution, the crystal was transferred into a large-volume crystallization drop [30 µl protein solution (40 mg ml^{-1}) was added to 30 µl reservoir solution as a sitting drop], which was pre-equilibrated against 1000 µl reservoir solution (15% PEG 400, 100 m*M* $MnCl_2$, 20 m*M* imidazole pH 7.0) overnight at 4°C. This crystal continued to grow and reached a final size of 4 × 1.3 × 0.7 mm (∼3.6 mm^3) in one month (Fig. 3*c*).

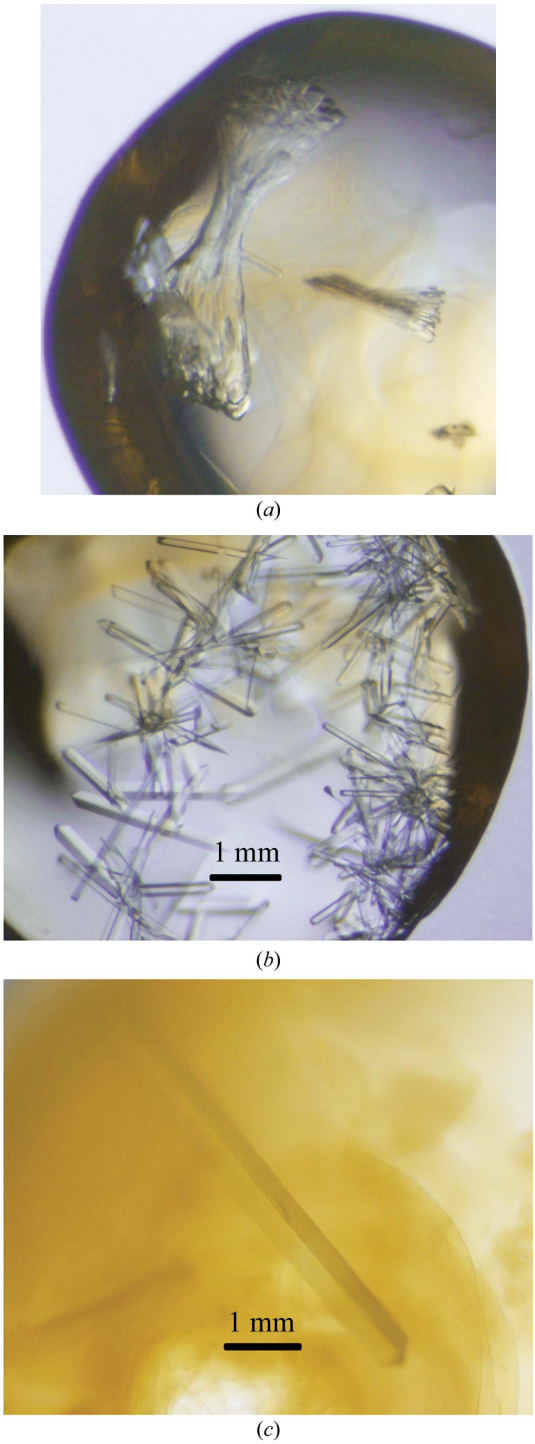

(*a*)

(*b*)

(*c*)

Figure 3
Crystallization of the ecDHFR–folate–$NADP^+$ complex. (*a*) *De novo* crystallization using the hanging-drop method. (*b*) Single crystals obtained using the microseeding technique. (*c*) The 4 × 1.3 × 0.7 mm (3.6 mm^3) size crystal obtained from the macroseeding technique.

Table 1
Data collection and processing.

Values in parentheses are for the highest resolution shell.

Data collection	Neutron	X-ray
Space group	$P2_12_12_1$	
Unit-cell parameters (Å, °)	a = 34.3, b = 45.7, c = 98.9, $\alpha = \beta = \gamma$ = 90	a = 34.3, b = 45.6, c = 99.0, $\alpha = \beta = \gamma$ = 90
Resolution (Å)	2.0	1.6
Unique reflections	8745	20795
Multiplicity	7.5 (5.8)	4.1 (4.0)
Completeness (%)	79.3 (61.3)	97.7 (94.0)
R_{merge}†	0.188 (0.305)	0.097 (0.446)
$\langle I/\sigma(I)\rangle$	5.3 (3.2)	13.7 (2.97)

† $R_{merge} = \sum_{hkl}\sum_i |I_i(hkl) - \langle I(hkl)\rangle| / \sum_{hkl}\sum_i I_i(hkl)$, where $I_i(hkl)$ is the measured intensity and $\langle I(hkl)\rangle$ is the mean intensity of all measured observations of reflection *hkl*.

2.3. Data collection and processing

The large crystal was mounted in a quartz capillary containing the same reservoir solution listed above except it was formulated in 100% D_2O (Fig. 4*a*). The labile H atoms were allowed to exchange with D by vapor diffusion for several weeks before starting data collection. Quasi-Laue neutron diffraction data were collected to 2.0 Å resolution at room temperature on the IMAGINE beamline (Meilleur *et al.*, 2013) located at HFIR (Oak Ridge National Laboratory, Oak Ridge, Tennessee, USA; Fig. 4*b*). The crystal was held stationary at a different φ setting for each exposure. A total of 33 images were collected with an average exposure time of 12 h per image from four different crystal orientations. The neutron data were processed using *LAUEGEN* (Campbell, 1995), which was modified to account for the cylindrical geometry of the detector (Campbell *et al.*, 1998). *LSCALE* (Arzt *et al.*, 1999) was used to determine the wavelength-normalization curve using the intensities of symmetry-equivalent reflections measured at different wavelengths. No explicit absorption corrections were applied. These data were then merged in *SCALA*, which is incorporated in the *CCP*4 program suite (Winn *et al.*, 2011). The statistics of the neutron data collection are shown in Table 1.

A small crystal obtained using the microseeding technique and appropriate for room-temperature X-ray diffraction was mounted and equilibrated against the D_2O-containing reservoir solution in the same fashion as the crystal used for neutron diffraction. The 1.6 Å resolution X-ray diffraction data were collected using a Rigaku HomeFlux X-ray diffractometer equipped with a MicroMax-007 HF X-ray generator, Osmic VariMax optics and an R-AXIS IV^{++} image-plate detector. The diffraction data were indexed, integrated and scaled using the *HKL*-3000 software suite (Minor *et al.*, 2006). The statistics of X-ray data collection are shown in Table 1.

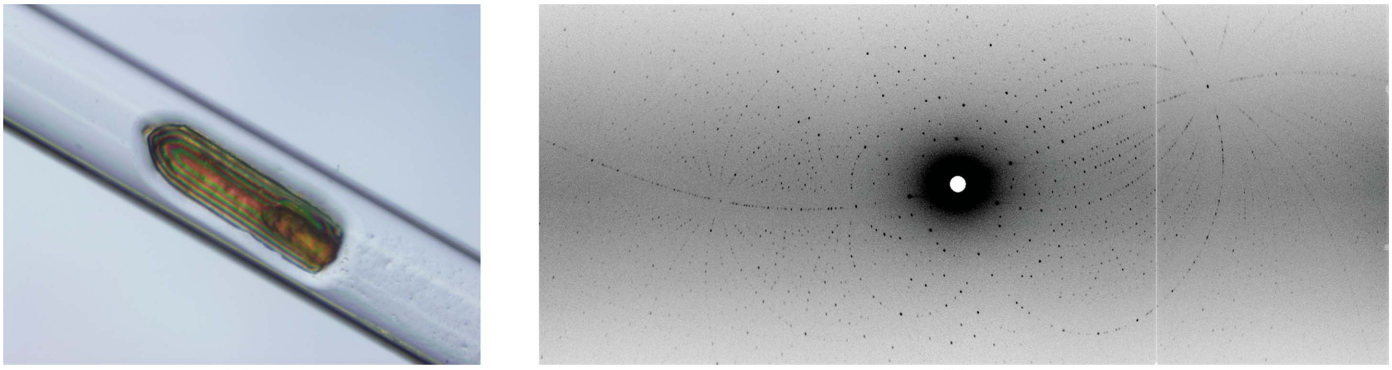

(*a*) (*b*)

Figure 4
Neutron data collection of the large ecDHFR crystal. (*a*) The crystal mounted in a quartz capillary. (*b*) A Laue neutron diffraction pattern of the crystal.

3. Results and discussion

Joint XN refinement (Adams *et al.*, 2009) of the ternary-complex structure is in progress utilizing *PHENIX* (Adams *et al.*, 2010), which allows the use of both the neutron and the X-ray data for complete structural refinement (Afonine *et al.*, 2010). The preliminary results show that D atoms exchanged on the amide backbone and many side chains were visible in the $2F_o - F_c$ and $F_o - F_c$ nuclear density maps. Owing to their incoherence and contribution to negative neutron scattering, chemically non-exchangeable H atoms at aliphatic and aromatic CH groups were detected as troughs in the $2F_o - F_c$ nuclear density map. Some dynamic side chains of residues, such as Lys and Arg, were not clear in the nuclear density map owing to the low data completeness, but are clearly visible in the electron-density map because of its higher resolution and data completeness. Detailed structural analysis of the ternary complex will be reported elsewhere.

The reaction catalyzed by DHFR has been studied in depth over the past 50 years using different spectroscopic, structural and theoretical methods. However, without direct observation of H atoms, the mechanistic details still remain controversial. Here, we used NC to study the structure of ecDHFR–folate–$NADP^+$ ternary complex, a pseudo model of the Michaelis complex. Elucidating the protonation states of the ligands, key catalytic residues and solvent molecules should be helpful to solve the longstanding puzzle.

To collect neutron diffraction data with reasonable resolution (higher than 2.2 Å) for H-atom identification and within a reasonable length of time, it is important to obtain a large crystal (>0.1 mm^3), one of the bottlenecks for NC (Blakeley *et al.*, 2008). We first used the microseeding technique to obtain small single crystals and then applied the macroseeding technique to enhance the three-dimensional growth of one crystal in a large volume of a pre-equilibrated crystallization drop. No other crystals appeared in the drop used for macroseeding; thus, the protein in solution in the equilibrated drop did not form new nucleations and was incorporated into the lattice of the single transferred crystal. We found that during the crystal transfer it is important to remove potential microcrystals by washing the seed thoroughly. Otherwise, these invisible crystals attached to the seed surface would become nuclei and consume free protein in the crystallization drop that would grow into larger crystals, thus not allowing the macroseed to grow to a large volume. As has been detailed previously, we also found that it is important to slightly decrease the precipitant concentration during seeding in order to prevent the appearance of new crystals (Bergfors, 2003).

The flux on currently available neutron beamlines is considerably lower than that of synchrotron X-ray beamlines or even in-house X-ray diffractometers. Thus, the time required for data collection can range from days to weeks (Niimura & Bau, 2008; Blakeley *et al.*, 2008; Bennett *et al.*, 2008). In this work, we limited the data collection to 33 frames (12 h per frame) to keep the total data-collection time to around two weeks (16.5 d). The overall data completeness is 79.3% and the data completeness of the highest resolution shell is 61.3% (Table 1). In this respect, the inclusion of the X-ray diffraction data (data completeness of 97.7 and 94.0% overall and for the highest resolution shell, respectively) in structure refinement was helpful for increasing the data-to-parameter ratio and also for improving the accuracy of the final model (Adams *et al.*, 2009; Table 1). Combined with the previous computational, structural and biophysical studies, we expect that the XN refined structure will provide new understanding of the reaction mechanism of DHFR.

This work was partly supported by the Center for Structural Molecular Biology supported by the US Office of Biological and Environmental Research, US Department of Energy, under FWP ERKP752. PL was partly supported by an NIH–NIGMS-funded consortium (R01GM071939) between ORNL and LBNL to develop computational tools for neutron protein crystallography. MAW is supported by NIH grant R01GM092999. This research used facilities sponsored by the Scientific User Facilities Division, Office of Basic Energy Sciences, US Department of Energy. QW was partly supported by grant 2013CXJ083 from Yangzhou University, China.

References

Adams, P. D. *et al.* (2010). *Acta Cryst.* D**66**, 213–221.
Adams, P. D., Mustyakimov, M., Afonine, P. V. & Langan, P. (2009). *Acta Cryst.* D**65**, 567–573.
Afonine, P. V., Mustyakimov, M., Grosse-Kunstleve, R. W., Moriarty, N. W., Langan, P. & Adams, P. D. (2010). *Acta Cryst.* D**66**, 1153–1163.
Arzt, S., Campbell, J. W., Harding, M. M., Hao, Q. & Helliwell, J. R. (1999). *J. Appl. Cryst.* **32**, 554–562.
Bajorath, J., Kraut, J., Li, Z. Q., Kitson, D. H. & Hagler, A. T. (1991). *Proc. Natl Acad. Sci. USA*, **88**, 6423–6426.
Bennett, B. C., Gardberg, A. S., Blair, M. D. & Dealwis, C. G. (2008). *Acta Cryst.* D**64**, 764–783.
Bennett, B., Langan, P., Coates, L., Mustyakimov, M., Schoenborn, B., Howell, E. E. & Dealwis, C. (2006). *Proc. Natl Acad. Sci. USA*, **103**, 18493–18498.
Bennett, B. C., Meilleur, F., Myles, D. A. A., Howell, E. E. & Dealwis, C. G. (2005). *Acta Cryst.* D**61**, 574–579.
Bennett, B. C., Xu, H., Simmerman, R. F., Lee, R. E. & Dealwis, C. G. (2007). *J. Med. Chem.* **50**, 4374–4381.
Bergfors, T. (2003). *J. Struct. Biol.* **142**, 66–76.
Bhabha, G., Tuttle, L., Martinez-Yamout, M. A. & Wright, P. E. (2011). *FEBS Lett.* **585**, 3528–3532.
Blakeley, M. P., Langan, P., Niimura, N. & Podjarny, A. (2008). *Curr. Opin. Struct. Biol.* **18**, 593–600.
Campbell, J. W. (1995). *J. Appl. Cryst.* **28**, 228–236.

Campbell, J. W., Hao, Q., Harding, M. M., Nguti, N. D. & Wilkinson, C. (1998). *J. Appl. Cryst.* **31**, 496–502.
Chen, Y. Q., Kraut, J., Blakley, R. L. & Callender, R. (1994). *Biochemistry*, **33**, 7021–7026.
Cummins, P. L. & Gready, J. E. (2001). *J. Am. Chem. Soc.* **123**, 3418–3428.
Falzone, C. J., Wright, P. E. & Benkovic, S. J. (1994). *Biochemistry*, **33**, 439–442.
Fisher, S. J., Blakeley, M. P., Cianci, M., McSweeney, S. & Helliwell, J. R. (2012). *Acta Cryst.* D**68**, 800–809.
Khavrutskii, I. V., Price, D. J., Lee, J. & Brooks, C. L. (2007). *Protein Sci.* **16**, 1087–1100.
Maharaj, G., Selinsky, B. S., Appleman, J. R., Perlman, M., London, R. E. & Blakley, R. L. (1990). *Biochemistry*, **29**, 4554–4560.
Meilleur, F., Munshi, P., Robertson, L., Stoica, A. D., Crow, L., Kovalevsky, A., Koritsanszky, T., Chakoumakos, B. C., Blessing, R. & Myles, D. A. A. (2013). *Acta Cryst.* D**69**, 2157–2160.
Minor, W., Cymborowski, M., Otwinowski, Z. & Chruszcz, M. (2006). *Acta Cryst.* D**62**, 859–866.
Niimura, N. (1999). *Curr. Opin. Struct. Biol.* **9**, 602–608.
Niimura, N. & Bau, R. (2008). *Acta Cryst.* A**64**, 12–22.
Reyes, V. M., Sawaya, M. R., Brown, K. A. & Kraut, J. (1995). *Biochemistry*, **34**, 2710–2723.
Sawaya, M. R. & Kraut, J. (1997). *Biochemistry*, **36**, 586–603.
Schweitzer, B. I., Dicker, A. P. & Bertino, J. R. (1990). *FASEB J.* **4**, 2441–2452.
Sharma, M. & Chauhan, P. M. (2012). *Future Med. Chem.* **4**, 1335–1365.
Shrimpton, P. & Allemann, R. K. (2002). *Protein Sci.* **11**, 1442–1451.
Sukumar, N., Mathews, F. S., Langan, P. & Davidson, V. L. (2010). *Proc. Natl Acad. Sci. USA*, **107**, 6817–6822.
Winn, M. D. *et al.* (2011). *Acta Cryst.* D**67**, 235–242.
Yuthavong, Y. *et al.* (2012). *Proc. Natl Acad. Sci. USA*, **109**, 16823–16828.